Electric-Field Switching of Magnetic Topological Charge in Type-I Multiferroics

Changsong Xu,[1] Peng Chen,[1] Hengxin Tan,[2] Yurong Yang,[3,4] Hongjun Xiang,[5,6,7,*] and L. Bellaiche[1,†]
[1]Physics Department and Institute for Nanoscience and Engineering, University of Arkansas, Fayetteville, Arkansas 72701, USA
[2]Max Planck-Institute of Microstructure Physics, Weinberg 2, 06120 Halle (Saale), Germany
[3]National Laboratory of Solid State Microstructures and Collaborative Innovation Center of Advanced Microstructures, Department of Materials Science and Engineering, Nanjing University, Nanjing 210093, China
[4]Jiangsu Key Laboratory of Artificial Functional Materials, Nanjing University, Nanjing 210093, China
[5]Key Laboratory of Computational Physical Sciences (Ministry of Education), State Key Laboratory of Surface Physics, and Department of Physics, Fudan University, Shanghai 200433, China
[6]Collaborative Innovation Center of Advanced Microstructures, Nanjing 210093, China
[7]Shanghai Qi Zhi Institute, Shanghai 200232, China

(Received 5 May 2020; accepted 17 June 2020; published 17 July 2020)

Applying electric field to control magnetic properties is a very efficient way for spintronics devices. However, the control of magnetic characteristics by electric fields is not straightforward, due to the time-reversal symmetry of magnetism versus spatial inversion symmetry of electricity. Such fundamental difficulty makes it challenging to modify the topology of magnetic skyrmionic states with electric field. Here, we propose a novel mechanism that realizes the electric-field (E) switching of magnetic topological charge (Q) in a controllable and reversible fashion, through the mediation of electric polarization (P) and Dzyaloshinskii-Moriya interaction (D). Such a mechanism is coined here EPDQ. Its validity is demonstrated in a multiferroic VOI_2 monolayer, which is predicted to host magnetic bimerons. The change in magnetic anisotropy is found to play a crucial role in realizing the EPDQ process and its microscopic origin is discussed. Our study thus provides a new approach toward the highly desired electric-field control of magnetism.

DOI: 10.1103/PhysRevLett.125.037203

Nanosized skyrmionic spin patterns (that have topological charges) have been intensively studied since they can lead to novel or efficient applications in advanced spintronics, e.g., high-density storage devices [1,2]. Besides skyrmions, a meron is another topological defect within the zoo of complex spin textures [3]. A meron can be viewed as a half skyrmion, with its hosting magnets having in-plane anisotropy [4,5]. Its rotational sense (vorticity) of the whirled spin patterns is determined by the Dzyaloshinskii-Moriya interaction (DMI) [6] in most cases. A single meron has half integer topological charge Q [4], as defined by $Q = 1/4\pi \int \mathbf{m} \cdot (\partial \mathbf{m}/\partial x) \times (\partial \mathbf{m}/\partial y) dxdy$ ($\mathbf{m}$ is the unit spin vector), in contrast with the integer Q of skyrmions. On the other hand, a pair of merons, also called a bimeron, regains integer values, namely, $Q = 0, \pm 1$, and tend to have lower energy than separated merons [5,7]. The sign of Q determines the direction of the transverse motion of electrons and holes in the topological Hall effect (THE) (where the Hall resistance is $\rho_{xy}^{\mathrm{THE}} = \rho_0 Q$) [5,8] and that of the skyrmionic particles in the skyrmion Hall effect [9,10].

A central concept for applications resides on the efficient manipulation of skyrmionic topological defects [24]. Many approaches, such as magnetic field pulse [25,26], spin polarized current [27,28], and thermal excitation [29,30], have been applied to control the morphology and mobility of such topological objects. Among them, the most energy conscious way is to apply an electric field, which is nearly dissipation-free. Pioneering works have established the electric-field creation and annihilation of skyrmions [31–35]. However, switching the sign of Q with the electric field remains theoretically challenging and experimentally unrealized. Here, we propose a mechanism that we coined EPDQ, which enables electric-field (E) switching of magnetic topological charge (Q) through the mediation of coupled polarization (P) and DMI (D), as illustrated in Fig. 1(a). We demonstrate that such an EPDQ mechanism can be realized in specific type-I multiferroics [36] where the proper ferroelectricity is induced by displacements of magnetic ions. The realization of the EPDQ mechanism is presently investigated in a candidate VOI_2 monolayer, which is found to possess coupled polarization and DMI, as well as, bimeron states.

VOI_2 is among the van-der-Waals layered multiferroic VOX_2 (X = Cl, Br, I) family [37–39]. A VOI_2 monolayer has been previously predicted to be ferromagnetic (FM) and ferroelectric (FE) [13]. Vanadium has a valence state of V^{4+} ($3d^1$) and its displacement along the x direction leads to electric polarization, which is proper in nature [see Figs. 1(c) and 1(d)] [40]. As shown in Figs. 1(b)–1(d), a VOI_2 monolayer consists of VO_2I_4 octahedra and contains V_2I_2 planes, which is reminiscent of the Cr_2I_2 plane in CrI_3,

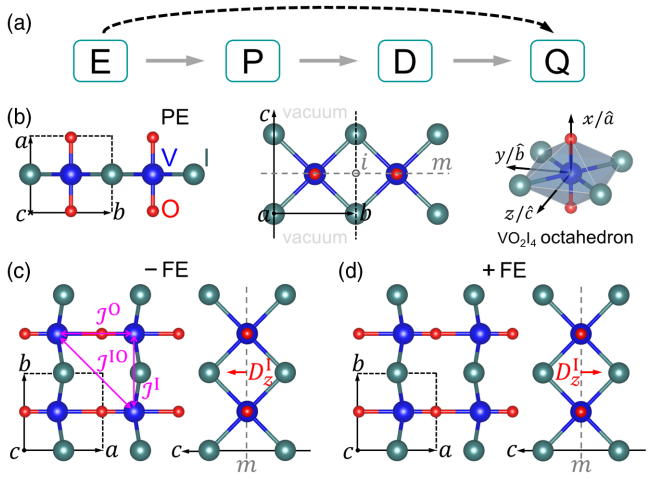

FIG. 1. Panel (a) illustrates the EPDQ mechanism. Panel (b) shows the PE *Pmmm* phase, as well as the VO_2I_4 octahedron. Panels (c) and (d) display the FE *Pmm*2 phases with opposite polarizations. $\mathcal{J}^{\mathrm{I}}$ and $\mathcal{J}^{\mathrm{O}}$ indicate the magnetic V-V interactions that are mediated by I and O, respectively, while $\mathcal{J}^{\mathrm{IO}}$ represents the diagonal V-V coupling. D_z^{I} is the DMI extracted from $\mathcal{J}^{\mathrm{I}}$. Grey letters i and m denote the inversion center and mirror plane, respectively. The $\boldsymbol{a}$, $\boldsymbol{b}$, and $\boldsymbol{c}$ lattice vectors are parallel to x, y, and z directions, respectively. The polarization lies along $\pm\boldsymbol{a}$ (or $\pm x$), which corresponds to the $\pm$FE state, respectively.

where the strong spin-orbit coupling (SOC) of I induces a strong Kitaev interaction [41,42]. In the paraelectric (PE) phase, an inversion center i is located in the middle of the V_2I_2 frame. In the FE phase, such an inversion center is lifted by the polar displacements of V, which then result in a significant DMI.

Density functional theory (DFT) calculations with the four-state method [14,15] are performed to obtain the magnetic exchange coupling parameters $\mathcal{J}^{\mathrm{I}}$, $\mathcal{J}^{\mathrm{O}}$, $\mathcal{J}^{\mathrm{IO}}$ [see Fig. 1(c)], as well as single ion anisotropy (SIA) coefficients $\mathcal{A}$, each in 3×3 matrix form (see Supplemental Material (SM) [11]). The nonzero elements of such matrices are adopted to construct the following spin Hamiltonian for the VOI_2 monolayer:

$$\mathcal{H} = \mathcal{H}^{\mathrm{DEC}} + \mathcal{H}^{\mathrm{DMI}} + \mathcal{H}^{\mathrm{SIA}}, \tag{1}$$

with

$$\mathcal{H}^{\mathrm{DEC}} = \sum_{\langle i,j\rangle^A}^{\mathrm{I,O,IO}} \sum_{\alpha}^{x,y,z} J^A_{\alpha\alpha} S_i^\alpha S_j^\alpha,$$

$$\mathcal{H}^{\mathrm{DMI}} = \sum_{\langle i,j\rangle^{\mathrm{I}}} \mathbf{D}^{\mathrm{I}} \cdot \mathbf{S}_i \times \mathbf{S}_j, \mathcal{H}^{\mathrm{SIA}} = \sum_i \sum_{\alpha}^{x,y} A_{\alpha\alpha} (S_i^\alpha)^2, \tag{2}$$

where $\mathcal{H}^{\mathrm{DEC}}$, $\mathcal{H}^{\mathrm{DMI}}$, and $\mathcal{H}^{\mathrm{SIA}}$ represent energies from diagonal exchange couplings (DECs), DMI, and SIA, respectively. The sum over $\langle i,j\rangle^A$, which denotes the $\mathrm{V}_i - \mathrm{V}_j$ pair bridged by A, runs through all first nearest neighbors (for A = I and O) and second nearest neighbors (for A = IO); the sum over i runs through all single V sites.

TABLE I. Magnetic parameters of VOI_2 in the −FE state. The superscript A of $J^A_{\alpha\alpha}$ is either I, O, or IO. $S = 1/2$ is adopted and the energy unit is meV.

(−FE)	I	O	IO
J^A_{xx}	−8.20	−5.35	−0.76
J^A_{yy}	−8.66	−5.29	−0.75
J^A_{zz}	−8.59	−5.20	−0.72
D^{I}_z 1.76		A_{xx} 0.01	A_{yy} 0.04

The obtained magnetic parameters are listed in Table I. All J's are negative, which is consistent with the predicted FM nature of the VOI_2 monolayer [13]. The anisotropy from $J^{\mathrm{I}}_{\alpha\alpha}$ is dominant and favors a FM state with magnetization lying along the y direction (FM-y), while that from $J^{\mathrm{O}}_{\alpha\alpha}$, $J^{\mathrm{IO}}_{\alpha\alpha}$, and SIA are weaker. We denote ϵ_x, ϵ_y, and ϵ_z the energies of the FM-x, FM-y, and FM-z states, respectively. One can then define the magnetic anisotropy energy (MAE) as $\varepsilon_y = \epsilon_y - (\epsilon_x + \epsilon_z)/2$, since $\epsilon_x \approx \epsilon_z$ in FE states. This definition yields $\varepsilon_y = -0.065$ meV/f.u. ("f.u." stands for formula unit) from the Hamiltonian of Eq. (2) and a similar value of $\varepsilon_y = -0.094$ meV/f.u. directly from DFT. Such good agreement attests to the accuracy of our magnetic parameters and the model Hamiltonian. Moreover, $\mathbf{D}^{\mathrm{I}}$ is found to only have a z component, which is in line with the Moriya's rule [6], indicating that the DM vector should be perpendicular to the mirror plane m passing through both V sites [see Figs. 1(c) and 1(d)]. The large value of $D^{\mathrm{I}}_z = 1.76$ meV is determined to arise from the strong SOC of the I element (see Fig. S1 of the SM [11]) and is likely to induce skyrmionic phases. Symmetry does not allow DMI in $\mathcal{J}^{\mathrm{O}}$ and the D^{IO}_z from $\mathcal{J}^{\mathrm{IO}}$ is negligibly small (<0.01 meV), indicating only collinear FM interaction along the x direction.

Parallel tempering Monte Carlo (PTMC) simulations [11] are then performed with the Hamiltonian of Eqs. (1) and (2) to determine low-energy phases. For the −FE phase [i.e., the FE state with negative polarization, see Fig. 1(c)], the ground state is determined to be a cycloid with its spins rotating in the ab plane [see Fig. 2(a)]. Such an in-plane cycloid propagates along the b axis in a clockwise manner with a period of $47b$ lattice constants [equivalently, 18.3 nm, see Fig. 3(a)]. Such a clockwise manner originates from the positive D^{I}_z. The energy of the $47b$-periodic cycloid is set as the zero reference hereinafter, and the FM-y state has a very low energy of 0.003 meV/f.u..

Isolated bimerons are further identified as metastable states. As shown in Fig. 2(b), each bimeron consists of two single merons imbedded in a FM-y background (note that bimerons are also found to coexist with cycloids in other states). The top bimeron has a core-up antivortex ($a\uparrow$) on

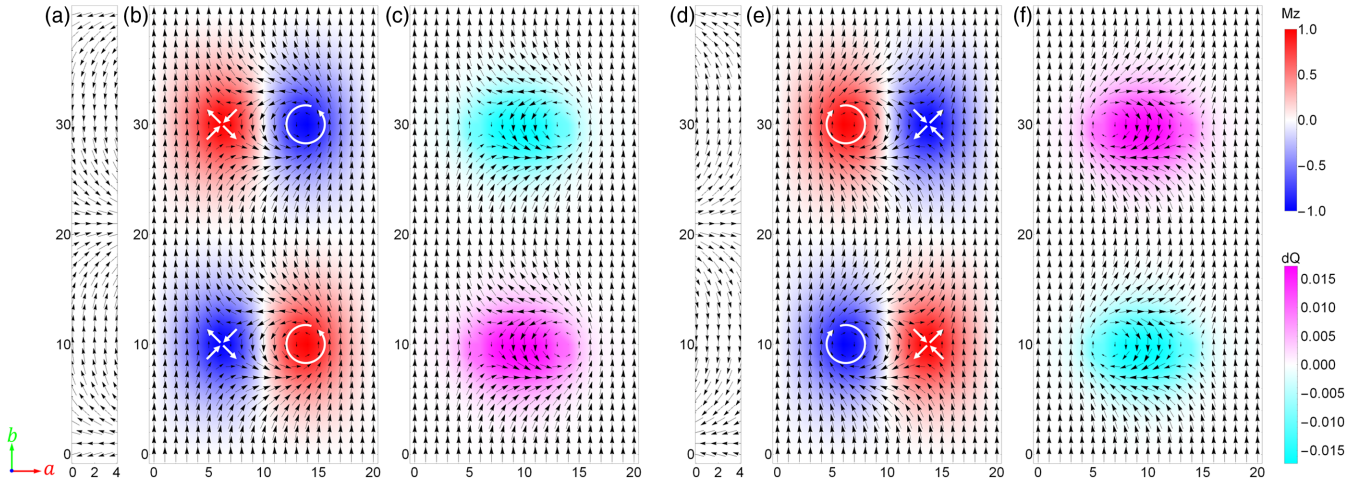

FIG. 2. Spin textures and distribution of topological charge Q. Panel (a) shows the ground state consisting of an in-plane cycloid. Panel (b) displays the spin textures made by two bimerons, with the black arrows being in-plane components while colors are assigned for out-of-plane components (polarity). The helicity and chirality of in-plane spin patterns are highlighted with white arrows. Panel (c) displays identical black arrows to (b), while the colors indicate the Q distribution. Panels (a)–(c) are for the −FE state, while panels (d)–(f) are the +FE. The spin textures shown here are from MC simulations that are followed by a conjugate gradient (CG) algorithm [11,12], which guarantees that all the predicted phases locate at their energy minimum.

the left and a core-down vortex ($v\downarrow$) on the right (the antivortex and vortex involve *in-plane* magnetic dipoles, while the wording "up" and "down" is used for out-of-plane components of the spins). In contrast, the bottom bimeron has a core-down antivortex ($a\downarrow$) on the left and a core-up vortex ($v\uparrow$) on the right. Such two kinds of bimerons, with the same in-plane patterns but different polarity, are mostly equally observed in the MC simulations. The cores of the two

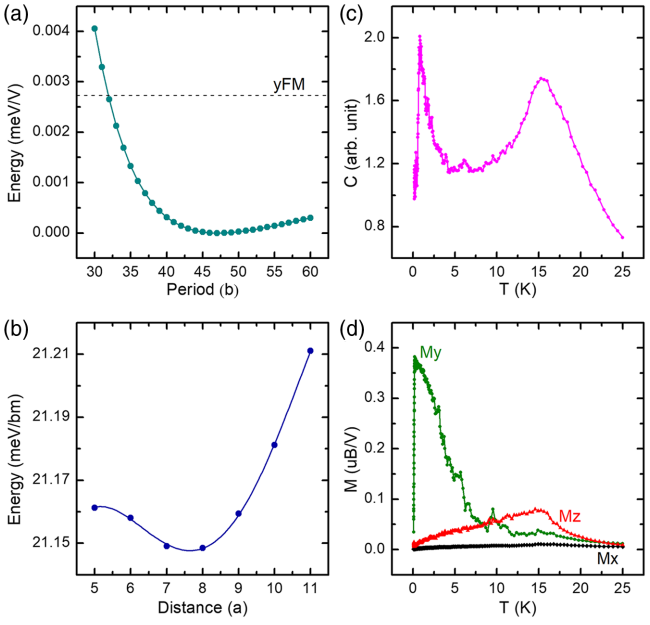

FIG. 3. Panel (a) shows the energy of a cycloid as a function of its period. Panel (b) displays the energy of bimerons as a function of meron core distance. Panels (c) and (d) show the temperature dependence of the specific heat and magnetization, respectively.

merons forming each bimeron are aligned along the x axis while the magnetic moments in the FM background are mostly along the perpendicular y direction. Such an arrangement results from the finite value of D_z^{I} and contrasts with cores of merons being aligned along the direction of the magnetic dipoles of the FM background in other systems (because, in that case, the DMI vector lies along a different direction) [5,12]. The cores of two merons in each bimeron are separated by a distance of $8a$ and the size of the bimeron yields $\sim 16a \times 10b$ (6.2×3.9 nm^2). Bimerons of such sizes are coined here as $16a \times 10b$ bimerons.

All the $16a \times 10b$ bimerons are degenerate with a low energy of 21.15 meV/bm ("bm" standing for bimeron). In order to reveal their microscopic origin, the total energy is decomposed into each term of Eq. (2). It is found that (i) D_z^{I} is responsible for the in-plane spin whirling and contribute to a major energy gain of −17.75 meV/bm; (ii) SIA favors out-of-plane spin components and leads to a minor energy gain of −1.06 meV/bm (note that neglecting $\mathcal{H}^{\mathrm{SIA}}$ does not affect the formation of bimerons); and (iii) all other terms cost energy. The chiral effects of DMI also lead to the fact that, for the −FE state, bimerons always have an antivortex on the left and a vortex on the right, which we denote as (a, v). On the other hand, meron cores are free to be up-down ($\uparrow$, $\downarrow$) or down-up ($\downarrow$, $\uparrow$), since the out-of-plane spin component is favored by SIA. Moreover, it is found that a bimeron with either a smaller or larger core distance than $8a$ has higher energy [see Fig. 3(b)]. The larger ones also allow ($\uparrow$, $\uparrow$) or ($\downarrow$, $\downarrow$) polarity (cf. Fig. S2).

The topological charge Q and its distribution are further studied. As shown in Fig. 2(c), the Q distribution is radial from a center, indicating that the $16a \times 10b$ bimeron can be considered to be a single particle. In contrast, if the two

merons are apart by a large distance, Q is distributed separately around each meron core, making it more like a correlated meron pair (see Fig. S2). Moreover, the topological charges of single merons follow the rule that $Q(a\downarrow) = Q(v\uparrow) = \frac{1}{2}$, while $Q(a\uparrow) = Q(v\downarrow) = -\frac{1}{2}$. Thus, the two bimerons in Fig. 2(c) exhibit $Q(a\uparrow, v\downarrow) = -1$ on the top and $Q(a\downarrow, v\uparrow) = 1$ at the bottom, while large distance meron pairs allow $Q(a\uparrow, v\uparrow) = Q(a\downarrow, v\downarrow) = 0$.

The temperature dependences of specific heat and magnetization are also studied. As shown in Fig. 3(c), the specific heat displays two major peaks, with one at $T_h = 15$ K and the other one at $T_l = 1$ K. Correspondingly and as shown in Fig. 3(d), M_z is maximized at T_h and M_y peaks at T_l, while M_x is nearly zero through the investigated temperature range. Let us understand such peaks by analyzing the magnetization characteristics of each state. The cycloid, as well as the $(\uparrow, \downarrow)$ and $(\downarrow, \uparrow)$ bimerons, results in zero magnetization along any direction, while FM-y leads to a saturated magnetization of $1\mu_B$ along the y direction. Bimerons with $(\uparrow, \uparrow)$ or $(\downarrow, \downarrow)$ polarity are the only source of net magnetization along z. Figures 3(c) and 3(d) can thus be interpreted to indicate that (i) spins begin to order at T_h, at which bimerons start to emerge; (ii) a mixing between FM-y and the cycloid reaches maximum at T_l, below which the ground state cycloid dominates (while, above T_l, the FM state is more predominant); and (iii) between T_l and T_h, cycloids with different periods, FM-y, bimerons with different sizes and polarities are found to coexist. Such coexistence is further evidenced by static spin structure factors $S(\boldsymbol{q})$, which also confirm bimerons as stable states below T_h (see SM for details [11]).

Let us now investigate electric-field effects. As shown in Fig. 4(a), our predicted polarization under zero field yields 68 μC/cm^2, which is very close to the reported 61 μC/cm^2 [13]. The electric hysteresis loop (P-E loop) is obtained from DFT via the method described in Refs. [43,44] that involves Born effective charges. The switch between the $-$FE and $+$FE states [Figs. 1(c) and 1(d)] is triggered by an electric field of 0.9 V/Å (note that atomistic approaches can overestimate electric field values by a factor of about 20 [45]). For each field-induced structure, we compute again the magnetic parameters by DFT, and find (see SM [11]) that the exchange couplings, J^{I}, J^{O}, and J^{IO}, keep the FM feature throughout the switching. In contrast, Fig. 4(b) reveals that D_z^{I} changes of sign when the polarization is reverted. It is also found that D_z^{I} linearly depends on polarization (with different slopes around the PE state and the FE ground states, respectively), which is reminiscent of the spin-current model, where $\mathbf{D}_{ij} \propto (\mathbf{e}_{ij} \times \mathbf{P})$ ($\mathbf{e}_{ij}$ is a unit vector pointing from site i to site j) [46,47]. Moreover, Fig. 4(c) indicates that the easy magnetic axis changes from the y direction near the FE ground states to the z direction near the intermediate PE state. The jumps in D_z^{I} and MAE, as shown in Figs. 4(b) and 4(c), can be explained by the different occupancies of t_{2g} orbitals of V^{4+} between FE and PE states [11].

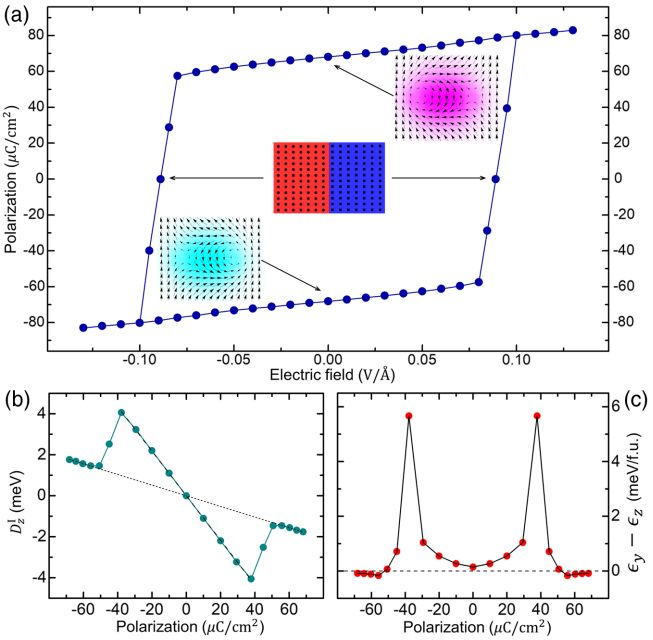

FIG. 4. Properties under electric fields. Panel (a) shows the P-E loop from DFT, with the insets indicating the spin patterns at different states from MC simulation (see Fig. 2 for color maps). Panels (b) and (c) display DMI parameter D_z^{I} and MAE $(\epsilon_y - \epsilon_z)$, respectively, as a function of polarization.

Let us look into effects of such polarization switching on magnetic topological charges, by starting with the $(a\uparrow, v\downarrow)$ bimeron in the $-$FE state (such a bimeron is a metastable state below T_h with an energy of 21.15 meV/bm above the ground state and thus should be accessible). For that, we run again PTMC simulations with the Hamiltonian of Eqs. (1) and (2), where the magnetic parameters are determined for each considered electric-field-induced structure. As the electric field increases along the opposite $+x$ direction, the $(\uparrow, \downarrow)$ polarity disappears in favor of up-down FM domains near the PE state as shown in the insets of Fig. 4(a), due to the out-of-plane anisotropy near the PE state. Further increasing the electric field flips the polarization towards $+$FE state. The reversed D_z^{I}, as well as the in-plane anisotropy, leads to the emergence of a $(v\uparrow, a\downarrow)$ bimeron in the $+$FE state, as shown in insets of Fig. 4(a). Comparing the bimerons in the $-$FE and $+$FE states shows that (i) the polarity keeps the same as $(\uparrow, \downarrow)$; (ii) the vortices become antivortices and *vice versa*; (iii) the right-handed chirality of the vortices in the $-$FE state turns to be left handed in the $+$FE state; and (iv) the antivortices revert their defining arrows [see Figs. 2(b) and 2(f)]. All these changes concomitantly lead to a switch of topological charge Q, since, e.g., for the top bimeron, the $-$FE state has $Q(a\uparrow, v\downarrow) = -1$, while the $+$FE state possesses $Q(v\uparrow, a\downarrow) = 1$. We thus obtain an electric-field control of magnetic topological charges, via our proposed EPDQ mechanism. Notably, in such an EPDQ mechanism, the electric field changes energy landscape by removing and

regaining DMI, so that the switching of topological charge does not need to overcome an energy barrier.

Note that the out-of-plane anisotropy near the PE state is crucial for the successful realization of the EPDQ process. It enables the formation of up-down FM domains, which is topologically trivial ($Q = 0$) but bridges nontrivial bimerons ($Q = -1$ and $+1$, respectively). The EPDQ process also requires a reversible-by-electric field polarization that normally has a proper character and that is closely related to the direction of the DMI. In that sense, it is similar to the magnetic chirality of cycloids predicted in type-I multiferroic $BiFeO_3$ when reverting the polarization by an electric field [47]. In contrast, a negative example is the type-II multiferroic Cu_2OSeO_3 (that has a polarization induced by chiral magnetism), for which the polarization and DMI cannot be switched by an electric field and, consequently, its skyrmionic states cannot be manipulated by electric fields [48]. Actually, the electromagnetic coupling in the present studied VOI_2, as well as its sister compound $VOBr_2$ [13,37], is an application of mirror symmetries in Moriya's rule [6]. Further utilization of the rotational symmetry to construct a similar EPDQ process in other polar magnets awaits to be explored.

In summary, the electric-field switch of magnetic topological charge is realized in multiferroic monolayer VOI_2 through a proposed EPDQ mechanism. VOI_2 is predicted to exhibit strong DMI and in-plane anisotropy, which stabilize the topologically nontrivial bimeron state. The EPDQ mechanism works in such a way that the electric field first flips the polarization and the sign of DMI, which then leads to a reversal topological charge of the bimerons. The EPDQ mechanism and the candidate VOI_2 thus have the possibility of impacting electric-field control of topological magnetism.

This work is supported by the Arkansas Research Alliance (Impact Grant) and the Vannevar Bush Faculty Fellowship (VBFF) from the Department of Defense. P. C. thanks ONR Grant No. N00014-17-1-2818. Y. Y. acknowledges the support from NSFC (11874207). H. X. is supported by NSFC (11825403, 11991061), Program for Professor of Special Appointment (Eastern Scholar), and Qing Nian Ba Jian Program. The Arkansas High Performance Computing Center (AHPCC) in University of Arkansas and HPCC in Nanjing University are also acknowledged.

*hxiang@fudan.edu.cn
†laurent@uark.edu

[1] A. Fert, V. Cros, and J. Sampaio, Skyrmions on the track, Nat. Nanotechnol. **8**, 152 (2013).
[2] A. K. Nayak, V. Kumar, T. Ma, P. Werner, E. Pippel, R. Sahoo, F. Damay, U. K. Rößler, C. Felser, and S. S. P. Parkin, Magnetic antiskyrmions above room temperature in tetragonal Heusler materials, Nature (London) **548**, 561 (2017).
[3] K. Everschor-Sitte, J. Masell, R. M. Reeve, and M. Kläui, Perspective: Magnetic skyrmionsoverview of recent progress in an active research field, J. Appl. Phys. **124**, 240901 (2018).
[4] X. Z. Yu, W. Koshibae, Y. Tokunaga, K. Shibata, Y. Taguchi, N. Nagaosa, and Y. Tokura, Transformation between meron and skyrmion topological spin textures in a chiral magnet, Nature (London) **564**, 95 (2018).
[5] B. Göbel, A. Mook, J. Henk, I. Mertig, and O. A. Tretiakov, Magnetic bimerons as skyrmion analogues in in-plane magnets, Phys. Rev. B **99**, 060407(R) (2019).
[6] T. Moriya, Anisotropic superexchange interaction and weak ferromagnetism, Phys. Rev. **120**, 91 (1960).
[7] X. Zhang, Y. Zhou, K. M. Song, T.-E. Park, J. Xia, M. Ezawa, X. Liu, W. Zhao, G. Zhao, and S. Woo, Skyrmion-electronics: Writing, deleting, reading and processing magnetic skyrmions toward spintronic applications, J. Phys. Condens. Matter **32**, 143001 (2020).
[8] Q. Shao, Y. Liu, G. Yu, S. Kwon Kim, X. Che, C. Tang, Q. L. He, Y. Tserkovnyak, J. Shi, and K. L. Wang, Topological Hall effect at above room temperature in heterostructures composed of a magnetic insulator and a heavy metal, National electronics review **2**, 182 (2019).
[9] W. Jiang, X. Zhang, G. Yu, W. Zhang, X. Wang, M. B. Jungfleisch, J. E. Pearson, X. Cheng, O. Heinonen, K. L. Wang *et al.*, Direct observation of the skyrmion Hall effect, Nat. Phys. **13**, 162 (2017).
[10] K. Litzius, I. Lemesh, B. Krüger, P. Bassirian, L. Caretta, K. Richter, F. Büttner, K. Sato, O. A. Tretiakov, J. Förster *et al.*, Skyrmion Hall effect revealed by direct time-resolved x-ray microscopy, Nat. Phys. **13**, 170 (2017).
[11] See Supplemental Material at http://link.aps.org/supplemental/10.1103/PhysRevLett.125.037203 for detailed methods and further discussions, which includes Refs. [2,12–23].
[12] C. Xu, J. Feng, S. Prokhorenko, Y. Nahas, H. Xiang, and L. Bellaiche, Topological spin texture in janus monolayers of the chromium trihalides $Cr(I,X)_3$, Phys. Rev. B **101**, 060404(R) (2020).
[13] H. Tan, M. Li, H. Liu, Z. Liu, Y. Li, and W. Duan, Two-dimensional ferromagnetic-ferroelectric multiferroics in violation of the d^0 rule, Phys. Rev. B **99**, 195434 (2019).
[14] H. Xiang, C. Lee, H.-J. Koo, X. Gong, and M.-H. Whangbo, Magnetic properties and energy-mapping analysis, Dalton Trans. **42**, 823 (2013).
[15] C. Xu, B. Xu, B. Dupé, and L. Bellaiche, Magnetic interactions in $BiFeO_3$: A first-principles study, Phys. Rev. B **99**, 104420 (2019).
[16] G. Kresse and D. Joubert, From ultrasoft pseudopotentials to the projector augmented-wave method, Phys. Rev. B **59**, 1758 (1999).
[17] A. V. Krukau, O. A. Vydrov, A. F. Izmaylov, and G. E. Scuseria, Influence of the exchange screening parameter on the performance of screened hybrid functionals, J. Chem. Phys. **125**, 224106 (2006).
[18] J. Sun, A. Ruzsinszky, and J. P. Perdew, Strongly Constrained and Appropriately Normed Semilocal Density Functional, Phys. Rev. Lett. **115**, 036402 (2015).
[19] Y. Miyatake, M. Yamamoto, J. J. Kim, M. Toyonaga, and O. Nagai, On the implementation of the 'heat bath' algorithms

for Monte Carlo simulations of classical heisenberg spin systems, J. Phys. C **19**, 2539 (1986).
[20] M. R. Hestenes and E. Stiefel, *Methods of Conjugate Gradients for Solving Linear Systems* (National Bureau of Standards, Washington, DC, 1952), Vol. 49.
[21] B. Berg and M. Lüscher, Definition and statistical distributions of a topological number in the lattice O(3) σ-model, Nucl. Phys. **B190**, 412 (1981).
[22] T. Okubo, S. Chung, and H. Kawamura, Multiple-q States and the Skyrmion Lattice of the Triangular-Lattice Heisenberg Antiferromagnet Under Magnetic Fields, Phys. Rev. Lett. **108**, 017206 (2012).
[23] L. Peng, R. Takagi, W. Koshibae, K. Shibata, K. Nakajima, T.-h. Arima, N. Nagaosa, S. Seki, X. Yu, and Y. Tokura, Controlled transformation of skyrmions and antiskyrmions in a non-centrosymmetric magnet, Nat. Nanotechnol. **15**, 181 (2020).
[24] N. Romming, C. Hanneken, M. Menzel, J. E. Bickel, B. Wolter, K. von Bergmann, A. Kubetzka, and R. Wiesendanger, Writing and deleting single magnetic skyrmions, Science **341**, 636 (2013).
[25] R. Hertel, S. Gliga, M. Fähnle, and C. M. Schneider, Ultrafast Nanomagnetic Toggle Switching of Vortex Cores, Phys. Rev. Lett. **98**, 117201 (2007).
[26] C. Moutafis, S. Komineas, and J. A. C. Bland, Dynamics and switching processes for magnetic bubbles in nanoelements, Phys. Rev. B **79**, 224429 (2009).
[27] F. Jonietz, S. Mühlbauer, C. Pfleiderer, A. Neubauer, W. Münzer, A. Bauer, T. Adams, R. Georgii, P. Böni, R. A. Duine *et al.*, Spin transfer torques in MnSi at ultralow current densities, Science **330**, 1648 (2010).
[28] X. Z. Yu, N. Kanazawa, W. Z. Zhang, T. Nagai, T. Hara, K. Kimoto, Y. Matsui, Y. Onose, and Y. Tokura, Skyrmion flow near room temperature in an ultralow current density, Nat. Commun. **3**, 988 (2012).
[29] L. Kong and J. Zang, Dynamics of an Insulating Skyrmion Under a Temperature Gradient, Phys. Rev. Lett. **111**, 067203 (2013).
[30] M. Mochizuki, X. Z. Yu, S. Seki, N. Kanazawa, W. Koshibae, J. Zang, M. Mostovoy, Y. Tokura, and N. Nagaosa, Thermally driven ratchet motion of a skyrmion microcrystal and topological magnon Hall effect, Nat. Mater. **13**, 241 (2014).
[31] J. S. White, K. Prša, P. Huang, A. A. Omrani, I. Živković, M. Bartkowiak, H. Berger, A. Magrez, J. L. Gavilano, G. Nagy *et al.*, Electric-Field-Induced Skyrmion Distortion and Giant Lattice Rotation in the Magnetoelectric Insulator Cu_2OSeO_3, Phys. Rev. Lett. **113**, 107203 (2014).
[32] P.-J. Hsu, A. Kubetzka, A. Finco, N. Romming, K. von Bergmann, and R. Wiesendanger, Electric-field-driven switching of individual magnetic skyrmions, Nat. Nanotechnol. **12**, 123 (2017).
[33] M. Schott, A. Bernand-Mantel, L. Ranno, S. Pizzini, J. Vogel, H. Béa, C. Baraduc, S. Auffret, G. Gaudin, and D. Givord, The skyrmion switch: Turning magnetic skyrmion bubbles on and off with an electric field, Nano Lett. **17**, 3006 (2017).
[34] J. S. White, I. Živković, A. J. Kruchkov, M. Bartkowiak, A. Magrez, and H. M. Rønnow, Electric-Field-Driven Topological Phase Switching and Skyrmion-Lattice Metastability in Magnetoelectric Cu_2OSeO_3, Phys. Rev. Applied **10**, 014021 (2018).
[35] P. Huang, M. Cantoni, A. Kruchkov, J. Rajeswari, A. Magrez, F. Carbone, and H. M. Rønnow, *In situ* electric field skyrmion creation in magnetoelectric Cu_2OSeO_3, Nano Lett. **18**, 5167 (2018).
[36] D. Khomskii, Trend: Classifying multiferroics: Mechanisms and effects, Physics **2**, 20 (2009).
[37] H. J. Seifert and J. Uebach, Beiträge zur chemie und struktur von vanadylhalogeniden, Z. Anorg. Allg. Chem. **479**, 32 (1981).
[38] H. Hillebrecht, P. J. Schmidt, H. W. Rotter, G. Thiele, P. Zönnchen, H. Bengel, H.-J. Cantow, S. N. Magonov, and M.-H. Whangbo, Structural and scanning microscopy studies of layered compounds MCl_3 (M = Mo, Ru, Cr) and $MOCl_2$ (M = V, Nb, Mo, Ru, Os), J. Alloys Compd. **246**, 70 (1997).
[39] H. Ai, X. Song, S. Qi, W. Li, and M. Zhao, Intrinsic multiferroicity in two-dimensional $VOCl_2$ monolayers, Nanoscale **11**, 1103 (2019).
[40] M. Stengel, C. J. Fennie, and P. Ghosez, Electrical properties of improper ferroelectrics from first principles, Phys. Rev. B **86**, 094112 (2012).
[41] C. Xu, J. Feng, H. Xiang, and L. Bellaiche, Interplay between Kitaev interaction and single ion anisotropy in ferromagnetic CrI_3 and $CrGeTe_3$ monolayers, npj Comput. Mater. **4**, 57 (2018).
[42] C. Xu, J. Feng, M. Kawamura, Y. Yamaji, Y. Nahas, S. Prokhorenko, Y. Qi, H. Xiang, and L. Bellaiche, Possible Kitaev Quantum Spin Liquid State in 2D Materials with $S = 3/2$, Phys. Rev. Lett. **124**, 087205 (2020).
[43] H. Fu and L. Bellaiche, First-Principles Determination of Electromechanical Responses of Solids Under Finite Electric Fields, Phys. Rev. Lett. **91**, 057601 (2003).
[44] L. Chen, C. Xu, H. Tian, H. Xiang, J. Íñiguez, Y. Yang, and L. Bellaiche, Electric-Field Control of Magnetization, Jahn-Teller Distortion, and Orbital Ordering in Ferroelectric Ferromagnets, Phys. Rev. Lett. **122**, 247701 (2019).
[45] B. Xu, J. Íñiguez, and L. Bellaiche, Designing lead-free antiferroelectrics for energy storage, Nat. Commun. **8**, 15682 (2017).
[46] H. Katsura, N. Nagaosa, and A. V. Balatsky, Spin Current and Magnetoelectric Effect in Noncollinear Magnets, Phys. Rev. Lett. **95**, 057205 (2005).
[47] S. Bhattacharjee, D. Rahmedov, D. Wang, J. Íniguez, and L. Bellaiche, Ultrafast Switching of the Electric Polarization and Magnetic Chirality in $BiFeO_3$ by an Electric Field, Phys. Rev. Lett. **112**, 147601 (2014).
[48] E. Ruff, P. Lunkenheimer, A. Loidl, H. Berger, and S. Krohns, Magnetoelectric effects in the skyrmion host material Cu_2OSeO_3, Sci. Rep. **5**, 15025 (2015).